ISSN 1063-7834, Physics of the Solid State, 2015, Vol. 57, No. 8, pp. 1559–1564. © Pleiades Publishing, Ltd., 2015.
Original Russian Text © A.D. Pogrebnjak, I.V. Yakushchenko, O.V. Bondar, O.V. Sobol', V.M. Beresnev, K. Oyoshi, H. Amekura, Y. Takeda, 2015, published in Fizika Tverdogo Tela, 2015, Vol. 57, No. 8, pp. 1529–1534.

MECHANICAL PROPERTIES, PHYSICS OF STRENGTH, AND PLASTICITY

Influence of Implantation of Au^- Ions on the Microstructure and Mechanical Properties of the Nanostructured Multielement (TiZrHfVNbTa)N Coating

A. D. Pogrebnjak[a, *], I. V. Yakushchenko[a], O. V. Bondar[a], O. V. Sobol'[b], V. M. Beresnev[c], K. Oyoshi[d], H. Amekura[d], and Y. Takeda[d]

[a] *Sumy State University, ul. Rimskogo-Korsakova 2, Sumy, 40007 Ukraine*

* *e-mail: alexp@i.ua*

[b] *National Technical University "Kharkiv Polytechnic Institute," ul. Frunze 21, Kharkiv, 61002 Ukraine*

[c] *Karazin Kharkiv National University, pl. Svobody 4, Kharkiv, 61022 Ukraine*

[d] *National Institute for Material Science (NIMS), 1 Chome-2-1 Sengen, Tsukuba, Ibaraki Prefecture, 305-0047 Japan*

Received February 9, 2015

Abstract—It has been found that the phase with the fcc lattice of the NaCl structural type is formed due to the vacuum-arc deposition of the nanostructured multicomponent (TiZrHfVNbTa)N coating. Implantation of negative Au^- ions with a dose of 1×10^{17} cm^{-2} leads to the formation of a disordered polycrystalline structure without a preferred orientation of the fcc phase and nanocrystallites from 5–7 to 1–3 nm is size, which are dispersed in a layer up to 35 nm in depth. Nanohardness increases to 33 GPa, and the Vickers hardness reaches 51 GPa. Gold nanoclusters are formed in the near-surface region, while the fcc lattice and the formation of local Au regions are observed in the coating itself. Fragments with the hcp lattice are formed at depths above 180 nm because of the low nitrogen concentration.

DOI: 10.1134/S1063783415080259

1. INTRODUCTION

The last decade is characterized by the development of a new class of high-entropy alloys (HEAs), which consist of at least five main components with the atomic concentration from 5 to 35%. The main feature of HEAs is that a single-phase stable substitutional solid solution is formed in them, preferentially with the fcc or bcc lattice, which is simultaneously thermodynamically stable and has a high strength (see, e.g., references in reviews [1, 2] and monograph [3]).

The preparation of nitrides or carbides from HEAs is also a very urgent problem of the modern materials science, because they are characterized by a higher oxidation resistance, wear resistance, and high hardness along with high plasticity as compared to "pure" HEAs. The problem of determining the limits of stability to implantation of nitrides deposited from HEAs is also very important, for which we selected negative Au^- ions with a dose up to 1×10^{17} cm^{-2} and a kinetic energy of 60 keV. Such a selection is substantiated by the fact that they can be more simply identified (for example, using the Rutherford backscattering spectroscopy (RBS) or proton-induced X-ray emission (PIXE)), as well as by the fact that most of elements of the high-entropy coating under study (Ti, Zr, Hf, Nb, Ta) do not interact with gold with the formation of intermetallic compounds.

2. EXPERIMENTAL TECHNIQUE

The phase composition of coatings was measured using X-ray diffractometers DRON-3M in CrK_α radiation and RINT-2500 V with the use of the position-sensitive proportional counter (PSPC/MDGT). The working voltage and current of the X-ray diffractometer were 40 kV and 300 mA, respectively. Measurements were performed at angles of 3°, 10°, and 30° for samples in the initial state (after coating deposition) and at angles of 2° and 10° for samples implanted by Au^- ions. The phase-structural state was investigated using a DRON-4 diffractometer in CuK_α radiation (wavelength $\lambda = 0.154178$ nm) using a graphite monochromator in the secondary beam. The diffraction spectrum for the phase analysis was recorded according to the scheme of θ–2θ scanning with the Bragg–Brentano focusing in an angle range of 25°–90°. Recording was performed in point-by-point mode with a scanning step $\Delta(2\theta) = 0.02°$–$0.2°$ and accumulation duration of pulses in each point of 10–100 s depending on the width and intensity of diffraction peaks. To analyze the elemental composition, we used two methods, namely, microanalysis with the help of energy-dispersive X-ray spectroscopy (EDX) using a JEOL-7000F scanning electron microscope (Japan) and secondary ion mass spectroscopy (SIMS) using an ULVAC-PHI TRIFT V nanoTOF time-of-flight spectrometer (Physical Electronics Inc., Japan). To inves-

Deposition parameters and elemental composition of the (TiZrHfVNbTa)N coatings under study

Sample no.	U, V	P_N, Torr	Concentration, at %						
			N	Ti	Zr	Hf	V	Nb	Ta
1	−150	3×10^{-3}	54	7.03	8.52	11.30	5.02	9.93	4.20
2	−150	3×10^{-4}	46	9.04	9.80	12.81	5.60	12.13	4.62
3	−150	7×10^{-4}	53	9.72	8.44	9.42	6.54	8.1	4.78
4	−70	7×10^{-4}	36	16.60	16.85	8.79	6.95	9.92	4.89
5	−70	4×10^{-3}	55	10.76	7.71	8.06	5.85	8.38	4.24
6	−70	5.2×10^{-3}	55	6.96	8.42	9.33	6.23	7.82	4.04
7	−70	0.5×10^{-4}	22	14.65	15.15	15.35	9.75	13.75	7.25
Cathode	–	–	–	21.52	18.77	15.5	10.2	18.2	15.81

tigate the distribution topography of elements over the surface, we used the RBS and PIXE methods with a 1.5-MeV proton microbeam of about 0.5 μm in diameter. To investigate the surface of multicomponent coatings, their elemental composition, and distribution of elements over the coating surface, we used a JSM-6010 LA scanning electron microscope with an energy-dispersive spectrometer (JEOL, Japan). Measurements were performed in a low vacuum at a working accelerating voltage of 20 kV.

Coatings were fabricated by vacuum-arc deposition with the target evaporation from a high-entropy alloy of the TiZrHfVNbTa system in the medium of nitrogen reactive gas. Deposition parameters are presented in the table, where U is a constant negative bias potential across the substrate and P_N is the pressure of the nitrogen atmosphere during the deposition; the current arc was varied insignificantly from 95 to 110 A, and the focusing current was varied from 0.4 to 0.5 A. We selected U of −70 and −150 V based on the preliminary investigations of similar coatings [4]. In contrast with [5], where nitride coatings were deposited from a five-element HEA, in this study we used the cathode of six elements and applied the pulsed deposition mode with the connection of a high-voltage pulsed generator [6], which allowed us to enhance the energy of the ion-plasma flux in the deposition instant, to improve coating adhesion to the substrate, and to fabricate more dispersed coating structure. Coatings up to 8 μm thick were deposited on steel discs 45 mm in diameter and 4 mm thick. Microhardness measurements were performed using a REVETEST device (Switzerland), while nanohardness and elastic modulus were investigated in a dynamic mode using a Triboindentor TI-950 device (HYSITRON, Inc.). The structure and phase composition were analyzed using transmission electron microscopy (TEM) and high-resolution transmission electron microscopy using a JEOL JEM-2100F electron microscope with the electron energy up to 200 keV, for which the foils were prepared using an ion beam.

Negative Au^- ions were generated by the Cs-assisted source of heavy ions of the plasma-sputtered type produced by Nissan High Voltage Co Ltd. An intense beam of negative ions was formed from two electrodes and accelerated to 60 keV (the current beam ≤4 mA).

3. RESULTS AND DISCUSSION

It is seen from the table that an increase in pressure from 3×10^{-4} to 3×10^{-3} Torr leads to a considerable increase in the nitrogen concentration in the coating composition. This is accompanied by a decrease in the content of such metallic elements as Ti, Nb, and V. The variation in pressure in a chamber during the deposition leads to the variation in concentrations of elements in the coating, which differ from that one characteristic of the composition of a cast cathode. The results obtained using EDS, RBS, and PIXE showed that the gold concentration is 2.1–2.2 at % at the projective path length of Au^- ions $R_p \approx 34$ nm.

Figure 1 shows the XRD spectra (XRD is the X-ray diffraction analysis) of high-entropy coatings deposited at various nitrogen pressures during the deposition. It is seen from the results of XRD analysis that the phase with the fcc lattice is formed as the main crystalline phase, which is characteristic of the nitride structure of the multielement alloy. The average crystallite size of the fcc phase in coatings at a low pressure of 3×10^{-4} Torr determined by the Scherrer equation is about 8 nm. In this case, the preferred growth orientation of crystallites with plane (200) parallel to the surface is formed (in this case, axis of texture [100] is perpendicular to the surface plane). According to the Vickers hardness investigations of coatings, a high hardness of 51 ± 0.7 GPa is observed in this case. Spectrum *2* in Fig. 1, which corresponds to the coating deposited at a comparatively high pressure of 3×10^{-3} Torr, has a fundamental difference: the preferred orientation of plane (111) parallel to the growth axis appears, which manifests itself in a form of an essential increase in relative intensity of peaks from the corre-

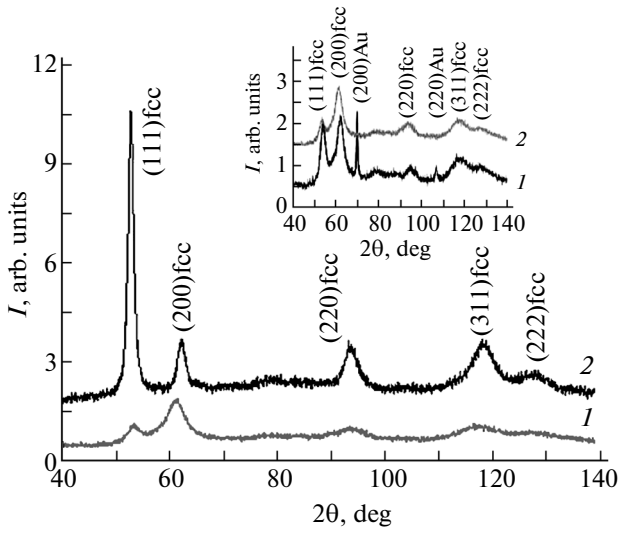

Fig. 1. Fragments of the diffraction spectra of the (TiZrHfVNbTa)N coatings deposited at different pressures $P_N = (1)\ 3 \times 10^{-4}$ and $(2)\ 3 \times 10^{-3}$ Torr. The inset shows the spectra recorded at $P_N = 3 \times 10^{-4}$ Torr after irradiation with Au^- ions (*1*) at a small incidence angle of 2° and (*2*) at a large constant incidence angle of 10°.

sponding plane. The average crystallite size of the fcc phase of the coating deposited at a higher pressure considerably increases being already 17–20 nm.

To investigate the implantation effect of Au^- ions, we used CrK_α radiation with a wavelength of 0.2285 nm, at which the depth of the informative layer in the case of the incidence angle of 2° is about 70 nm (which is comparable with the projective path depth R_p). Parameter R_p for this coating, according to our calculations, was about 34 nm.

Inset to Fig. 1 shows the diffraction spectra measured at an incidence angle of 10° (which gives the information on the material bulk 0.5 μm thick) and 2° (which gives the information on the state of the surface layer up to 70 nm thick). It is seen that the ion implantation of Au^- with a dose of 1×10^{17} cm^{-2} leads to the largest disorder and formation of polycrystalline structure without the preferred orientation in the near-surface region. In this case, the appearance of the peaks, which correspond to the planes of implanted gold by their position, is noted.

The comparison of crystallite sizes shows that as the depth of the informative layer decreases, the average crystallite size of multielement nitride decreases from 7.2 nm (at a depth up to 0.5 μm) to 5 nm in the layer, into which Au^- ions implanted (by projective path depth R_p and somewhat deeper).

Figure 2a shows the results of the dynamic indentation of the Berkovich pyramid (triboindenter [2, 4]), and a two-dimensional (top inset) and three-dimensional (bottom inset) imprint images, starting from

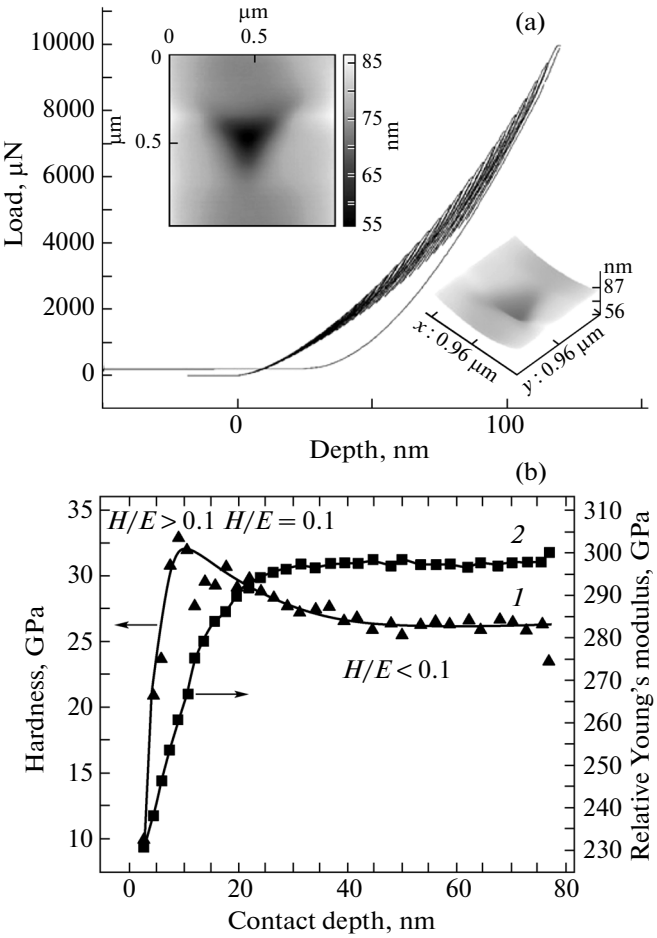

Fig. 2. Results of mechanical studies of sample no. 6. (a) Indentation of the Berkovich pyramid under dynamic loading and (b) dependences of (*1*) nanohardness and (*2*) reduced elastic modulus on the penetration depth.

which, we can evaluate the indentation depth and determine the reduced elastic modulus. The measurements were performed upon varying the load to indenter from 500 to 10000 μN for sample no. 6. Figure 2b shows the corresponding dependences of nanohardness and reduced elastic modulus E_r on the penetration depth for a mode presented in Fig. 2a. An increase in nanohardness almost to 33 GPa is observed in the layer 30–35 nm thick, where implantation took place, with the gradual attainment of a horizontal line to the penetration depth of 80 nm. An increase in plasticity index in the implanted region also should be noted: $H/E \geq 0.1$, which points to excellent wear resistance. We can affirm that the implantation of heavy Au^- ions with the concentration up to 2.1–2.2 at % leads to an increase in the hardness almost by 15–20% and an increase in plasticity index higher than 0.1. These results confirm the results of measurements of nanohardness of the (ZrTaNbTiW)N high-entropy alloy under the plasma ion implantation of nitrogen ions with a dose from 0.8×10^{16} to 2×10^{17} cm^{-2} [7].

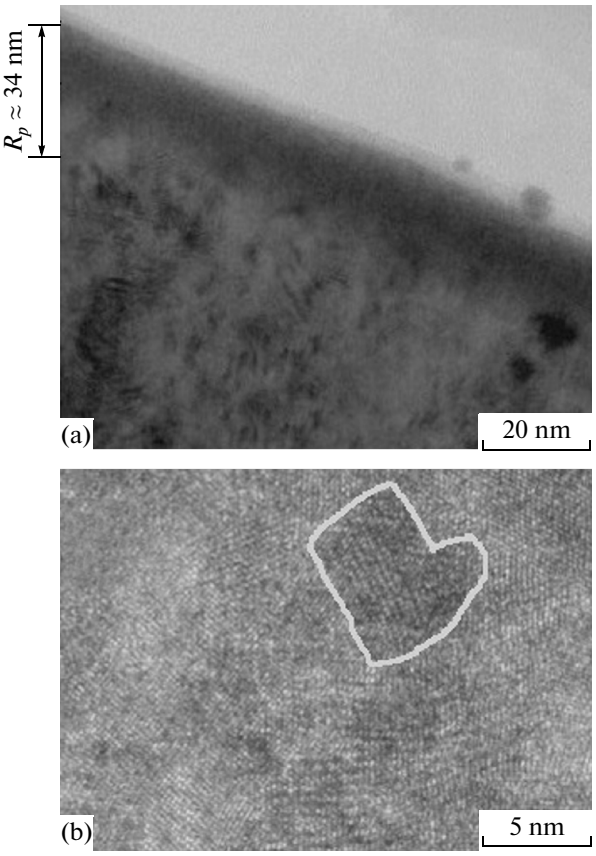

Fig. 3. TEM images of sections of the (TiZrHfVNbTa)N coating. (a) Near-surface layer with the indicated implantation depth and (b) fragment of the coating located at a depth of about 50 nm.

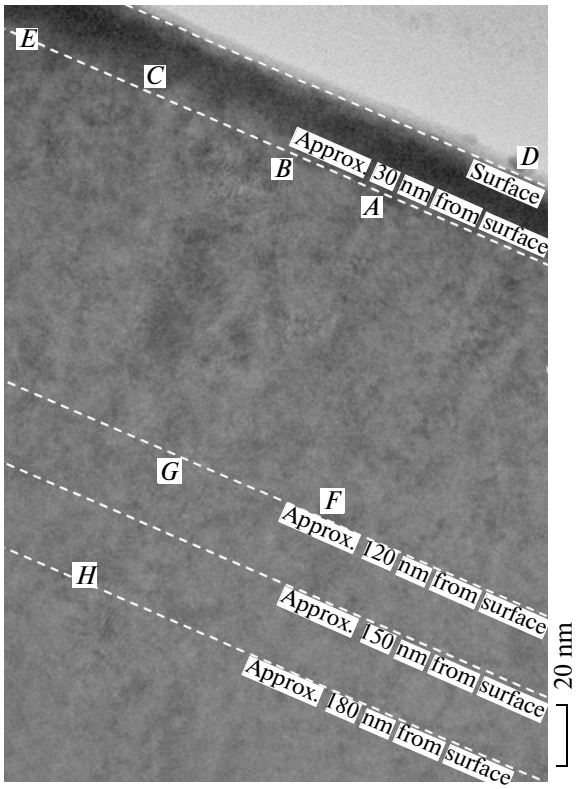

Fig. 4. Lateral section of sample no. 2 with marked investigation places.

The further increase in the implantation dose to 4×10^{17} cm^{-2} leads to a decrease in hardness and plasticity index.

The obtained values of the Vickers hardness are higher than nanohardness H and elastic modulus for coatings fabricated form nitrides of high-entropy alloy. This is associated with the fact that nanoindentation is performed in the static mode, while the Vickers hardness is determined in the static mode.

It should be noted that Au^- ions have high sputtering coefficient [8, 9]. Therefore, N atoms are partially sputtered from the surface under the high-dose implantation because of their weaker bond. A high density of individual cascades of displaced atoms (substitutional solid solution) is formed during the implantation, and defects are formed with high efficiency [9, 10]—vacancy-type and interstitial-type loops. Implanted Au^- ions in the coating form spherical nanocrystallites several nanometers in size (as it was shown for the implantation of Cu^- and Au^- ions into SiO_2 in [11]). The efficiency of recombination of point defects in the nanostructured coating increases near interfaces (nanograin interfaces, double or triple joints of nanograins) [12]. In addition, the percentage of interfaces during the implantation with heavy ions increases due to refining (crushing) the nanograins from 8 to 5 nm and smaller, due which, the disordered polycrystalline structure without the preferred orientation of the fcc phase is formed. Thus, deposited nanostructured coatings possess considerably higher resistance against the irradiation by Au^- ions compared with single crystals and polycrystals [9, 10].

Figure 3a shows the element of section of the (TiZrHfVNbTa)N coating implanted by Au^- ions to the concentration of 2.1 at % with energy of 60 keV. It is seen that the surface layer to depth $R_p \approx 34$ nm is disordered and has a polycrystalline structure close to amorphous-nanocrystalline one. Below this layer, a nanocrystalline structure with a nanograin size of about 7 nm is located (Fig. 3b). A bright line marks a nanograin about 7 nm in size located at a depth slightly lower than the implantation depth. At the same time, we can note by the TEM results that the nanograin sizes substantially decrease in the layer, in which the implantation occurred, and reach ~0.8–1 nm. As for the crystallite sizes obtained from the XRD data according to the Scherrer formula, these are the averaged values over the layer up to 70 nm thick.

To visualize the results of investigations, let us present the transmission microscopy data. Figure 4

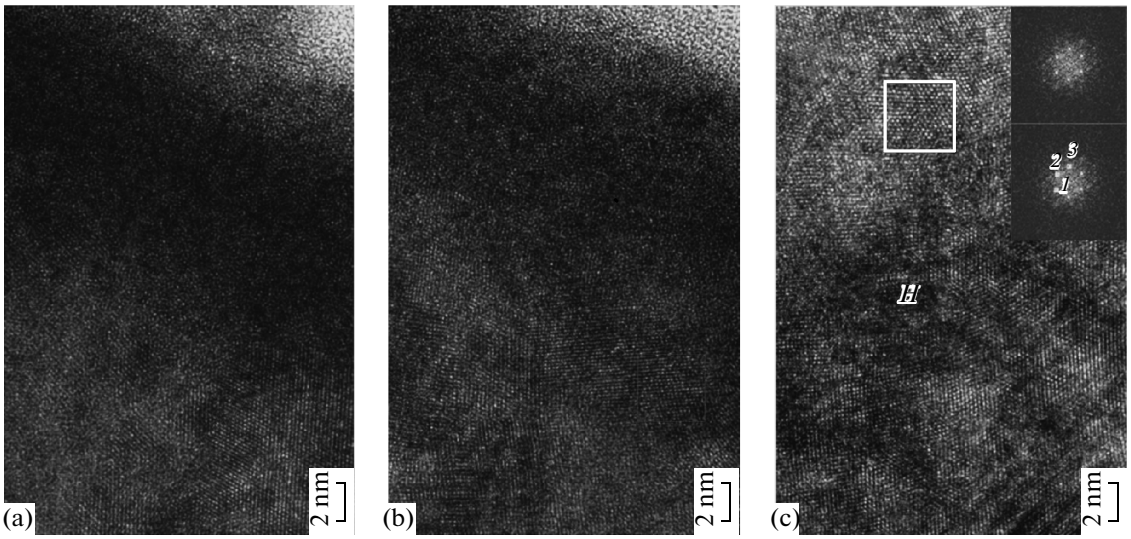

Fig. 5. Results of the electron microscopy investigation of sample no. 2. (a) In the surface region (zone *D*), (b) in the near-surface region at a depth of 20–30 nm (zone *E*), and (c) in the coating at a depth of 180 nm (the results of microdiffraction from the fragment limited by square are presented in the right upper corner).

shows the lateral section of the coating, on which the investigation places are marked; the diffraction vector is parallel to the surface plane.

Figure 5 shows the high-resolution electron microscopy images. Planes and their break at the boundaries are clearly seen in these images. It is seen that the average crystallite size is 5–7 nm, which agrees well with the results obtained by broadening the X-ray diffraction curves.

Interplanar distances for various fragments, which were determined starting from the microdiffraction data, show that the reflections from the planes with the fcc lattice having interplanar distances 0.250 nm (plane (111)) and 0.221 nm (plane (200)) manifest themselves in the near-surface region (zone *D* in Figs. 4 and 5a). This is somewhat lower than the data obtained from the position of the peaks of X-ray diffraction spectra, according to which, we obtained values of 0.257 nm (plane (111)) and 0.225 nm (plane (200)).

The feature of the near-surface zone, which is located at a depth of 20–30 nm from the surface (zone *E* in Figs. 4 and 5b), is the additional reflection at microdiffraction with an interplanar distance of 0.197 nm. Comparing these results with the data of low-angle radioscopy (inset in Fig. 1), we can assume that its appearance is associated with the presence of local regions based on implanted gold in the zone under consideration, for which the interplanar distance of 0.197 nm corresponds to plane (200).

An increase in the interplanar distance to 0.255–0.259 nm (plane (111)) and 0.226 nm (plane (200)) is observed in the region of deeper layers, i.e., to the values close to those for the bulk material according to the X-ray diffraction data. The appearance of reflections with the interplanar distance of 0.275–0.278 nm is observed at a depth of 180 nm (zone *H* in Figs. 4 and 5c). It is known that fcc an hcp crystal lattices are close by their internal energy with a sufficiently small energy barrier for the transformation. It is also known that the interplanar distance of 0.275–0.278 nm for nitrides of transition metals with the hcp lattice corresponds to plane (100). In connection with this, we can assume that the fcc lattice can transform into the hcp lattice in local regions of the coating material according to the shear mechanism due to the composition nonuniformity at a relatively low nitrogen content associated with a low working pressure. The driving force of this process can be the high thermodynamic stability of the hcp lattice with the lack of nitrogen atoms in octahedral interstices.

ACKNOWLEDGMENTS

This study was supported by budget programs no. 0112U001382 and 0113U000137, as well as by the International Program for Scientific Collaboration under the support of the Ministry of Education and Science of Ukraine no. 514 (between the Sumy State University and NIMS, Tsukuba, Japan).

REFERENCES

1. Y. Zhang, T. T. Zuo, Z. Tang, M. C. Gao, K. A. Dahmen, P. K. Liaw, and Z. P. Lu, Prog. Mater. Sci. **61**, 1 (2014).

2. A. D. Pogrebnjak, A. A. Bagdasaryan, I. V. Yakushchenko, and V. M. Beresnev, Russ. Chem. Rev. **83** (11), 1027 (2014).

3. B. S. Murty, J. W. Yeh, and S. Ranganathan, *High-Entropy Alloys* (Butterworth–Heinemann, Oxford, 2014).
4. A. D. Pogrebnjak, I. V. Yakushchenko, G. Abadias, G. P. Chartier, O. V. Bondar, V. M. Beresnev, Y. Takeda, O. V. Sobol', K. Oyoshi, A. A. Andreyev, and B. A. Mukushev, J. Superhard Mater. **35** (6), 356 (2013).
5. A. D. Pogrebnjak, V. M. Beresnev, D. A. Kolesnikov, M. V. Kaverin, A. P. Shipilenko, K. Oyoshi, Y. Takeda, R. Krause-Rehberg, and A. G. Ponomarev, Tech. Phys. Lett. **39** (3), 280 (2013).
6. A. D. Pogrebnjak, D. Eyidi, G. Abadias, O. V. Bondar, V. M. Beresnev, and O. V. Sobol, Int. J. Refract. Met. Hard Mater. **48**, 222 (2015).
7. X. Feng, G. Tang, X.Ma, M. Sun, and L. Wang, Nucl. Instrum. Methods Phys. Res., Sect. B **301**, 29 (2013).
8. A. D. Pogrebnjak, I. V. Yakushchenko, A. A. Bagdasaryan, O. V. Bondar, R. Krause-Rehberg, G. Abadias, P. Chartier, K. Oyoshi, Y. Takeda, V. M. Beresnev, and O. V. Sobol, Mater. Chem. Phys. **147** (3), 1079 (2014).
9. F. F. Komarov, *Ion Implantation into Metals* (Metallurgiya, Moscow, 1990) [in Russian].
10. A. D. Pogrebnjak, S. N. Bratushka, V. M. Beresnev, and N. Levintant-Zayonts, Russ. Chem. Rev. **82** (12), 1135 (2013).
11. N. Kishimoto, V. T. Gritsyna, Y. Takeda, C. G. Lee, and T. Saito, Nucl. Instrum. Methods Phys. Res., Sect. B **141**, 299 (1988); N. Kishimoto, V. T. Gritsyna, Y. Takeda, C. G. Lee, and T. Saito, J. Surf. Sci. **4**, 220 (1998).
12. V. Ivashchenko, S. Veprek, A. Pogrebnjak, and B. Postolnyi, Sci. Technol. Adv. Mater. **15** (2), 025007 (2014).

Translated by N. Korovin